Letters in Applied NanoBioScience
Open-Access Journal (ISSN: 2284-6808)

Article
Volume 12, Issue 4, 2023, 114
https://doi.org/10.33263/LIANBS124.114

DFT Calculation for Newly Synthesized 2-Chloro-1-(3-methyl-3-mesityl-cyclobutyl)– ethanone

Pelin Koparir [1], Rebaz Anwar Omar [2,*]

[1] Forensic Medicine Institute, Department of Chemistry, Firat University, 23169 Elazig, Turkey; mpelin23@hotmail.com (P.K.);
[2] Department of Chemistry, Faculty of Science & Health, Koya University, Koya KOY45, Kurdistan Region – F.R. Iraq; rebaz.anwar@koyauniversity.org (R.A.O.);
* Correspondence: e rebaz.anwar@koyauniversity.org (R.A.O.);

Scopus Author ID 56429205800

Received: 7.04.2022; Accepted: 17.05.2022; Published: 18.09.2022

Abstract: The synthesis of cyclobutane rings, particularly stereospecifically, poses significant challenges in synthetic chemistry due to the highly strained ring topologies. The cyclobutane-containing natural products are appealing targets for total synthesis due to their new chemical structures and exceptional biological activity. In this study, we have presented the synthesis and structure analysis of 2-chloro-1-(3-methyl-3-mesityl-cyclobutyl)–ethanone. The molecular elucidation was conducted by Fourier transform infrared (IR) and Nuclear magnetic spectroscopy (NMR). The I recording in 4000-500cm^{-1} was done in the potassium bromide solid phase, while the NMR for both Hydrogen and Carbon was done in the Dimethyl sulfoxide-6. Density functional theory (DFT) was used to stimulate and confirm the structure and molecular characterization. Using DFT/cc-pVDZ method to study various conformers of the compound and their minimum energies by the scanning potential energy surface. In addition, the molecular electrostatic potential map (MEP) and charge spreading have been plotted for the molecule to account for the chemical reactivity and site selectivity. Furthermore, the thermodynamic properties of the molecule have been studied. A good correlation was found between experimental and stimulation studies for Fourier transform infrared and Nuclear magnetic spectroscopy results. In the stimulation data, the conformer's energy differences were very small.

Keywords: cyclobutane; density functional theory; molecular electrostatic potential map; molecular reactivity; thermodynamic properties.

1. Introduction

Cyclobutane [1,2] $(C_2H_4)_2$ (CYLB) is an alicyclic compound that has Van der Walls interaction and is a polar molecule. CYLB is colorless, flammable, and water-insoluble; the boiling point is 12°C and the melting point is -80 ^{0}C. CYLB has no commercial and biological importance, but its complex derivatives are very good in biology and biotechnology. For example, 3-substituted cyclobutane carboxylic acid derivatives exhibit anti-inflammatory and antidepressant activity [3,4]. The effect of light on Diel-Alder reaction CYLB may be formed [5,6]. In 1887 William Perkin succeeded in synthesizing CYLB-carboxylic acid, the first generalized CYLB derivative [7]. Akhmedov et al. were; synthesized 1,1,3-trisubstituted cyclobutane rings from unsaturated derivatives with lewis acids [8,9]. Recently, many researchers synthesized and characterized CYLB derivatives [10-12]. Density functional theory (DFT) calculation has a reasonable cost-accuracy ratio for structure analysis in large

systems [13-16]; however, the calculations are always prohibitive and work best for charged systems [17-21]. The combination of DFT calculation and experimental studies leads to understanding the characterization of the molecule [22-25]. DFT has higher accuracy [26,27] in molecular analysis, including vibrational frequencies, thermodynamic, and electronic properties for a polyatomic molecule [28-31]. This study's main objective is to characterize the synthesis and molecular characterization of 2-chloro-1-(3-methyl-3-mesityl-cyclobutyl)–ethanone. DFT on the cc-pVDZ basis set has been used as a stimulation model of the molecule properties.

2. Materials and Methods

All chemicals, including; Ether $(C_2H_5)_2O$, $CaCl_2$ (anhydrous), $AlCl_3$ (anhydrous), KOH, $Na_2Cr_2O_7$, H_2SO_4, and DMSO-d6 were purchased from Merck and later used without extra purifications. 6-Chloro-4,5-epoxy-2-methyl-1-hexene was received from the organic Lab at Chemistry Department, Firat University, and it was distilled before use. Fourier transform infrared (FT-IR) spectra were recorded with the Perkin-Elmer spectrum. The melting point was measured using Electrothermal 9100. Nuclear magnetic spectroscopy (^{1}H-NMR and ^{13}C-NMR) spectra were recorded on Bruker ascend 400 NMR spectrometer operating at 400 MHz for ^{1}H and 100 MHz for ^{13}C NMR, using Dimethyl sulfoxide-6 (DMSO-d_6) as a solvent.

2.1. Synthesis of 2-chloro-1-(3-mesityl-3-methylcyclobutyl)ethan-1-ol.

The experimental setup was four nicks round bottom flask attached with a dropping funnel, thermometer, and calcium chloride tube placed in a mechanical mixer. After that, 1500 ml of mesitylene and 167 g of anhydrous $AlC1_3$ were added, followed by the addition of 183 g of epoxide compound dropwise at (11-12) ^{0}C. The mixture was stirred for 2 hours and then decomposed with 15% HCI. the solution was neutralized with a 5% NaOH aliquot. After that was dried with $MgSO_4$, and the solvent was removed from the rotary evaporator. Finally, 247 g of compound2-chloro-1-(3-mesityl-3 methylcyclobutyl) ethan-1-ol (3).

2.2. Synthesis of 2-chloro-1-(3-methyl-3-mesityl-cyclobutyl)–ethanon.

Four-neck conical flask 1000ml fitted with thermometer, funnel, stirrer and condenser, then sodium dichromate (0.29 mol), 2-chloro-1-(3-methyl-3-(2,4,6-trimethyl cyclohexyl) cyclobutyl) ethan-1-ol (0.52 mol) were added, followed by 50 ml water. H2SO4 (75 ml) (68% v/v) was added after 7-8 h running the experiment at room temperature from the neck of the funnel. The mixture was stirred for 18h at room temperature. The solid product was formed and filtered, and then the filtrate was extracted with several portions of diethyl ether. The extracts were combined and dried over anhydrous CaCl2, then recrystallized with ethyl alcohol as compound 4.

2.3. Characterization of 2-chloro-1-(3-methyl-3-mesityl-cyclobutyl)–ethanone.

The reaction illustrated in Figure 1 yielded, 55% of synthesis of 2-chloro-1-(3-mesityl-3-methylcyclobutyl)ethan-1-one. Molecular characteristics were; melting point: 97-98 ^{0}C; FT-IR (KBr, cm^{-1}, υ): 1812 (C=O), 1658 and 1612 (C=C in ring), 3155 (Ar-H); ^{1}H-NMR (400 MHz, DMSO-d_6, δ, ppm): 1.49 (s,3H, -CH3-(cyclobutane), 2.14 (s, 9H, -CH3 (mesitylene), 2.35-2.51 (m, 4H, -CH2)- (cyclobutane), 3.46 (p, 1H, -CH- (cyclobutane), J = 8.80 Hz), 4.55

(s, 2H, CH2-Cl), 6.71 (s, 2H, Ar-H); ^{13}C-NMR (100 MHz, DMSO-d_6, δ, ppm): In the spectrum drawn by ATP method, (5 peaks for CH3 AND CH2 s), (20.45, 20.75, 25.24, 37.68, 130.29); (7 pieces of CH and aprotic carbons), 39.77, 40.21, 48.42, 130.29, 134.06, 143.94, 203.90 Elemental analysis (theoretical): C, 72.57; H, 7.99; 0, 6.04; experimental, C, 72.56; H, 8.01; O, 6.07.

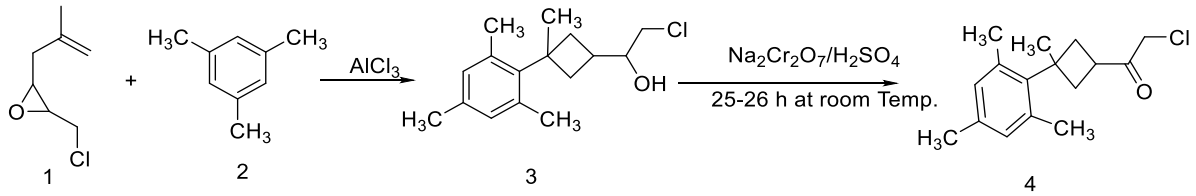

Figure 1. The mechanism of synthesizing compounds (4).

3. Results and Discussion

3.1. Computational study.

All theoretical calculations were carried out with Gaussian 09, using a combined approach of B3LYP and cc-pVDZ. First, the optimization and the vibrational frequency are confirmed for synthesizing 2-chloro-1-(3-mesityl-3-methylcyclobutyl) ethan-1-one. Second, NMR chemical shift was measured using the Gauge Independent Atomic Orbital (GIAO) process. Finally, Frontier molecular orbital, which is produced by the highest occupied molecular orbital" and "lowest unoccupied molecular orbital (HOMO-LUMO) energy level, molecular electrostatic potential (ESP) [32,33], atomic charge density, and thermodynamic properties were calculated [19,34].

3.2. Results and discussion molecular geometry.

The basis set of B3LYP/cc-pVDZ calculated bond lengths, bond angles, and dihedral angles of 2-chloro-1-(3-mesityl-3-methylcyclobutyl)ethan-1-one. Atomic numbering configuration of the theoretical geometric structure using ChemBioDraw and Gaussian View, presented in Figure 2. The aromatic ring was skewed from the natural hexagon, the bond length for C-C and C=C was equal to 1.39A^0 and 1.42A^0, respectively, but the actual bond length between C-C and C=C in the benzene ring was equal to 1.34A^0 and 1.54A^0 respectively. This variation of bond length is due to the steric effect of the -CH_3 groups in a present compound 4. The real bond length between C-C in cyclobutane was identical to 1.55A^0 [35,36], but in the current study assigned to 1.57A^0, the cyclobutane ring was attached by three different groups.

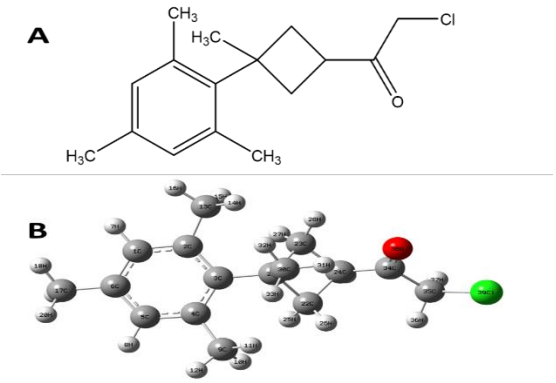

Figure 2. The geometrical structure of compound 4 a) Draw by ChemBioView Ultra b) Optimization by Gaussian.

Based on the result of the bond length for C=O and C-Cl, we can conclude that our data is comparable with previous data. The DFT calculations provide a narrowing angle of C3-C2-C1, C4-C3-C2, C5-C4-C3, and C6-C1-C2 by 119.85, 117.89, 119.88, and 122.55, respectively. The normal angle for the benzene ring is 1200. This distortion is caused by replacing the CH3 group at positions C2, C4, and C6 with the long chain in position C3. The variation in bond lengths, bond angles, and dihedral angles are summarized in Table 1.

Table 1. The geometrical optimization parameters include Bond Length, Bond angle, and Dihedral angle of compound 4 in the ground state.

Symbol	**Bond Length**	**Symbol**	**Dihedral angle**
C2-C1	1.40	C4-C3-C2-C1	-5.28
C3-C2	1.42	C5-C4-C3-C2	5.30
C4-C3	1.42	C6-C1-C2-C3	1.38
C5-C4	1.40	C9-C4-C3-C2	-172.76
C6-C1	1.39	C13-C2-C1-C6	-176.94
C9-C4	1.51	C17-C6-C1-C2	-178.07
C13-C2	1.51	C21-C3-C2-C1	178.71
C17-C6	1.50	C22-C21-C3-C2	-142.98
C21-C3	1.53	C23-C21-C3-C2	-41.28
C22-C21	1.57	C24-C21-C3-C2	-129.82
C23-C21	1.57	C34-C24-C23-C21	-105.53
C24-C23	1.54	C35-C34-C24-C23	-167.50
C34-C24	1.51	O38-C34-C24-C23	13.16
C35-C34	1.53	Cl39-C35-C34-C24	-171.27
O38-C34	1.21		
Cl39-C35	1.79		
Symbol	Bond Angle		
C3-C2-C1	119.85		
C4-C3-C2	117.89		
C5-C4-C3	119.88		
C6-C1-C2	122.55		
C9-C4-C3	123.83		
C13-C2-C1	116.27		
C17-C6-C1	121.53		
C21-C3-C2	120.87		
C22-C21-C3	116.96		
C23-C21-C3	117.28		
C24-C21-C3	91.34		
C34-C24-C23	116.32		
C35-C34-C24	113.27		
O38-C34-C24	123.93		
Cl39-C35C34	114.10		

C: is Carbone

3.2.1. NMR spectroscopy.

The basis set of B3LYP/ccpVDZ was used to stimulate ^{1}H- and ^{13}C-NMR spectra of compound 4; as the experimental approach, DMSO was used as a solvent. There were several identical peaks in the 1H- and 13C-NMR spectra of compound 4, as shown in Figures 3 and 4. Protons in the benzene ring are the first, and the most characteristic peaks appeared at 6.75 ppm for both H7 and H8. The second characteristic peak is the two methyl groups on the benzene ring; they are doublet peaks at 2.36ppm, with a higher intensity including six carbon, the. Finally, two hydrogen peaks (H36 and H37) were shifted to a lower field, meaning higher ppm (4.55ppm); also, the computing analysis was confirmed at 5.6ppm. All of the 1H-NMR shifts and characteristics were shown in Table 2 for both experimental and theoretical calculations.

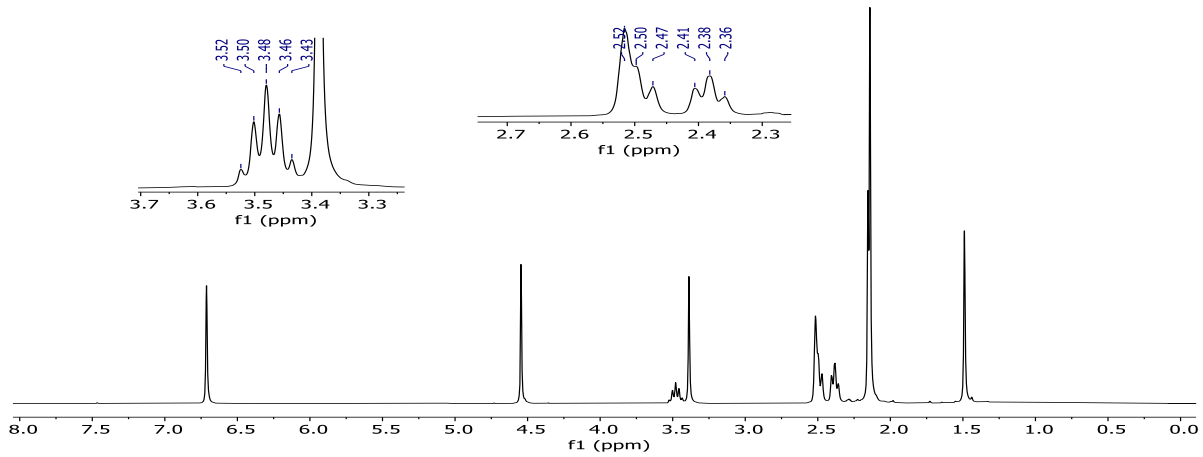

Figure 3. [1]H-NMR spectra of the compound 4.

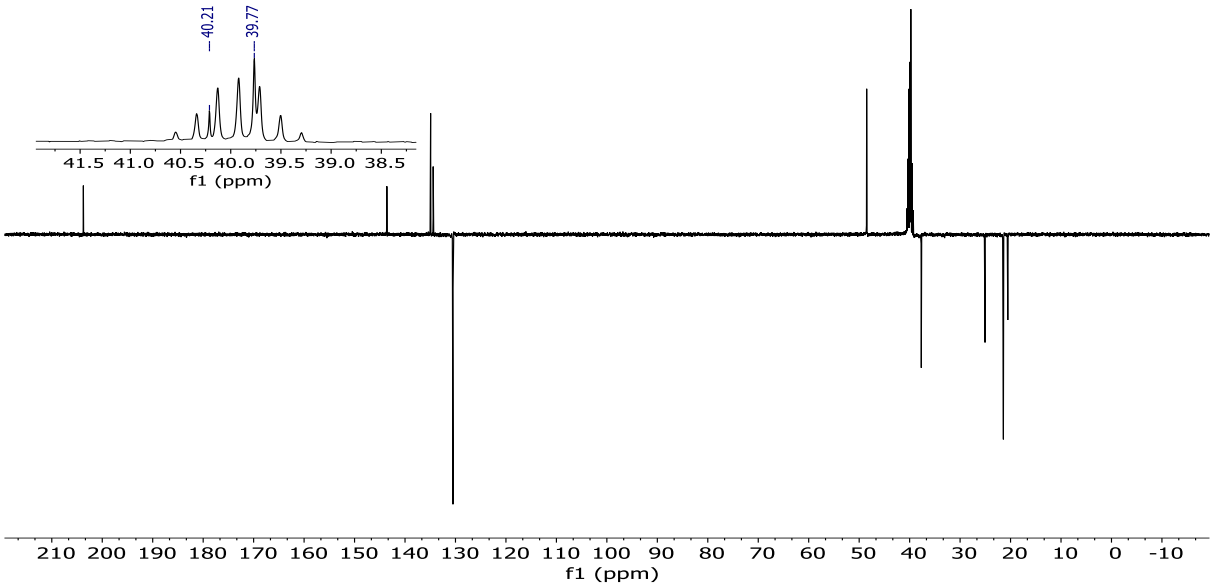

Figure 4. [13]C-NMR spectra of compound 4.

In the [13]C-NMR spectra, carbons of the three methyl groups (-CH_3) attached to the benzene ring were recorded experimentally at 20.75, 20.75, 20.45ppm, and the basis set computed the same range of shifts at 30.47, 30.28, 28.91 ppm, respectively. The carbonyl group (C=O) was recorded at 203.90ppm and 211.06ppm experimentally and theoretically, respectively. The aromatic carbon in the benzene ring experimentally appeared around 143.94ppm and theoretically appeared at 143.41ppm, as the electronegativity of the chlorine atom and carbonyl group of C35 were shifted to lower filed higher ppm (48.42ppm) and (64.38ppm) for experimentally and theoretically, respectively. All of the experimental and theoretical [13]C-NMR shifts and characteristics were summarized in Table 3., In general, there was a good agreement between experimental and theoretical data for compound 2-chloro-1-(3-mesityl-3-methylcyclobutyl)ethan-1-one, evidencing the applicability of the basis set to stimulate the molecular characteristics.

Table 2. Experimental and theoretical chemical shifts (ppm) of 1H-NMR of compound 4.

H number	Experimental Results (E)	Theoretical Results (T)
H7	6.75	7.9454
H8	6.75	7.9344
H36	4.55	5.6299
H37	4.55	5.4293

H number	Experimental Results (E)	Theoretical Results (T)
H25	3.52	4.1904
H29	3.50	4.1215
H28	3.48	3.7701
H27	3.46	3.7569
H15	2.52	3.7267
H10	2.52	3.6703
H19	2.52	3.6196
H14	2.36	3.3122
H20	2.41	3.2968
H18	2.50	3.2499
H11	2.47	3.1944
H26	3.43	3.1628
H31	2.41	3.1372
H16	2.38	3.1165
H12	2.37	3.0702
H32	1.5	2.4748
H33	1.5	2.4182

Table 3. Experimental and theoretical chemical shifts (ppm) of ^{13}C-NMR of compound 4.

C number	Experimental Results (E)	Theoretical results (T)
C34	203.90	211.06
C3	143.94	152.64
C2	143.94	143.41
C4	143.94	143.31
C6	134.06	142.40
C1	130.29	135.81
C5	130.29	135.68
C35	48.42	64.38
C21	40.21	54.66
C22	39.77	49.08
C24	39.77	47.19
C23	37.68	44.68
C30	25.24	33.55
C13	20.75	30.47
C9	20.75	30.28
C17	20.45	28.91

3.2.2. FT-IR spectroscopy.

In the FT-IR measurements for synthesis compounds 2-chloro-1-(3-methyl-3-mesityl-cyclobutyl)–ethanone, an identical peak appeared at 1745cm^{-1} for C=O. In addition, the peaks for the aromatic benzene ring were recorded at 1658,1612 cm^{-1}. The basis set stimulated the molecular vibration for CO, CH, and CH3 in a very close range to the experimental result, experimental and theoretical FT-IR spectra presented in Figure 5.

3.2.2.1. CO vibrations.

The two strong vibrations were observed in IR for CO groups, one is C-O stretching vibrations in a region 1250-850 cm^{-1} [37], and the second vibration is C=O at 1650- 1850 cm^{-1} [38,39]. The basis set of B3LYP/ccpVDZ recorded a very high infrared absorption band at 1812cm^{-1}.

3.2.2.2. CH and CH3 vibrations.

In the FT-IR spectra, the aromatic structures usually display multiple bands between 3000 and 3100 cm^{-1}, a characteristic region for vibration stretching C-H [39-41]. The experimental C-H stretching vibration was observed at 3022-3155 cm^{-1}; the same vibration was

calculated theoretically at 3156-3012 cm^{-1} using the B3LYP/ccpVDZ method, thus showing a strong correlation between the experimental and theoretical data, Table 4.

The CH group normally generates four fundamental bending vibrations, which are scissoring and rocking, wagging, and twisting (in-plane bending) (out-of-plane bend), respectively. Out-of-plane bending vibrations of C-H appeared in the 1000-675 cm^{-1} region, and in-plane bending vibrations of C-H appeared in the 1400-1050 cm^{-1} region [42]. The C-H ring vibrations in-plane bending appeared at 1396-1036cm^{-1} experimentally while theoretically appeared at 1398-1033cm^{-1}. The C-H out-of-plane ring bending vibrations appeared experimentally at 1276-1268 cm^{-1} and theoretically at 1265-1225 cm^{-1}. The CH_3 group typically generates nine fundamental vibrations, such as three modes of bending, three modes of stretching, two modes of rocking, and a single mode of torsion. The methyl group's symmetric and asymmetric stretching vibrations usually occur at 2850-3000 cm^{-1} [43]. In the area of 1650, 1156, and 1132 cm^{-1}, the aromatic ring carbon-carbon (C=C) stretching modes appeared; however, in theoretical, they appeared at 1658,1612, 1154, and 1132cm^{-1}. The difference between measured and observed frequencies was due to; the phase of the compound being measured as the experimental results belong to the solid phase and the theoretical calculations belong to the gaseous phase, and the experimental values reported in the presence of intermolecular interactions, while the calculations were performed on a single molecule.

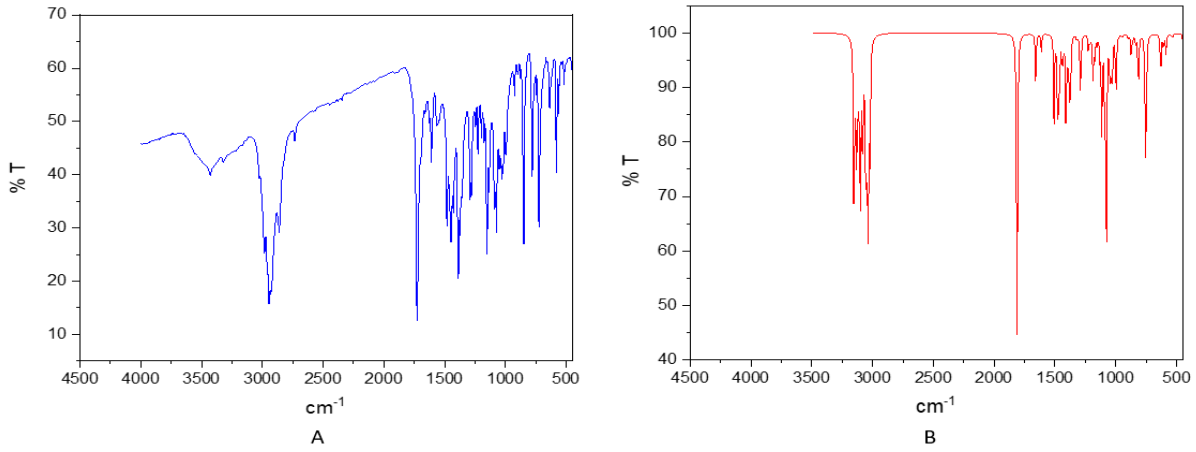

Figure 5. FT-IR spectra of compound 4 A) Practical B) Theoretical.

Table 4. Comparison of the experimental and theoretical vibrational spectra of compound 4.

Assignments With TED	Unscaled Frequencies (6-311(d, p)) B3LYP	FT-IR (cm^{-1}) With KBr	Assignments With TED	Unscaled Frequencies (6-311(d,p)) B3LYP	FT-IR (cm^{-1}) With KBr
υsC1H7,C5H8	3155	3156	υsC-Hring	1507	1508
υasC23H27,H28	3147	3148	υCH3	1481-1463	1484-1460
υasC22H25, H26	3134	3140	ScC17,H18,H20	1459,1049	1452
υasC13H14,H16	3133	3132	υC35,H37	1409	1412
υasC9H11,H12	3130	3124	υsCH3	1404	1404
υasC30H31H32	3126	3116	υs-inCH3-ring	1398,1046,1033	1396, 1036
υasC35H36,H37	3114	3108	ro-inC24H29	1376	1372
υasC17H18,H20	3112	3100	υasC-ring	1321,1316	1324
υasC30H32,H33	3102	3092	roC35H36,H37	1289	1284
υasC13H15,H16	3099	3084	υs-ouC23H27,H28	1274	1276
υsC9H10,H12	3098	3076	υsouC1H7,C5H8	1265	1268
υsC17H18,H20	3083	3068	roC23H27,C24H29	1261,1225	1260
υsC23H27,H28	3078	3060	υC21C23	1154	1156
υsC35H36,H37	3061	3052	υsC21C22,C23C24	1132	1132
υsC22H25,H26	3055	3044	υasC22C2324	999,996	996, 988
υsC13H14,H15,H16	3039	3036	υasC1C5C6	974	972

Assignments With TED	Unscaled Frequencies (6-311(d, p)) B3LYP	FT-IR (cm^{-1}) With KBr	Assignments With TED	Unscaled Frequencies (6-311(d,p)) B3LYP	FT-IR (cm^{-1}) With KBr
υsC9H10,H11,H12	3037	3028	υasC21C23C30	943	940
υsC30H31,H32,H33	3034	3020	υasC21C22C23	909,883	908
υsC17H18,H19,H20	3022	3012	roC22H25H26	815	884
υC=O	1812	1745	υsC35Cl39	753	756
υsC=C-ring	1658,1612	1650			

υ, stretching; s, symmetric; as, asymmetric; ro, rocking; ou, out of the plan; in, in a plan sc, scissorin

3.2.3. Molecular reactivity report.

Multiple factors were founded based on the HOMO and LUMO energy bandgap levels [15]. The ionization potential ($I=-E_{HOMO}$) is the least amount of energy available in a gaseous state to remove an electron from the atom or molecule. The quantity of discharge energy is called electronic affinity ($A=-E_{LUMO}$) when one electron is attached to the gaseous molecule. Electronegativity $\chi= (I + A)/2$ is the tendency of an atom to attract electrons. Weight transfer in a molecule is denoted by chemical hardness = (I - A)/2. The HOMO and LUMO energy values are also used to evaluate other reactivity descriptors, such as potential chemical $\mu= -\chi$, softness $s= 1/2\eta$, and global electrophilicity index = $\mu2/2\eta$ [44,45]. Usually, the chemical activity of the compound is shown by the energy values of HOMO and LUMO and the energy difference.

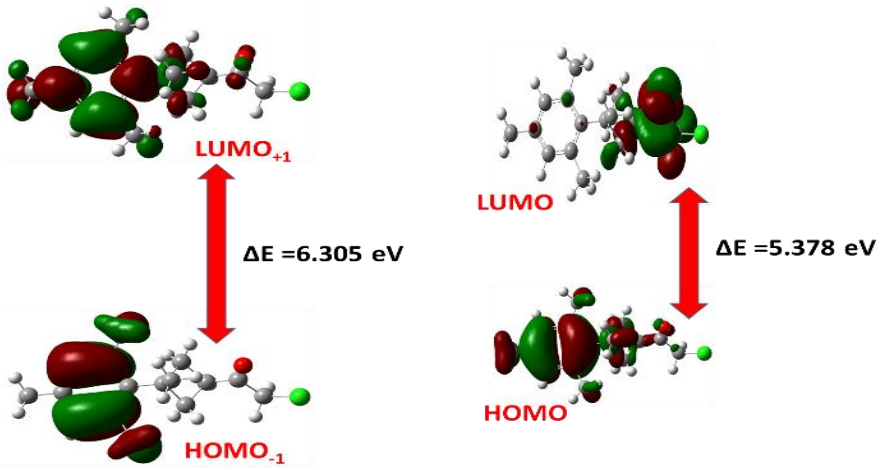

Figure 6. Molecular orbital and energy levels of compound 4 calculated by B3LYP/cc-pVDZ.

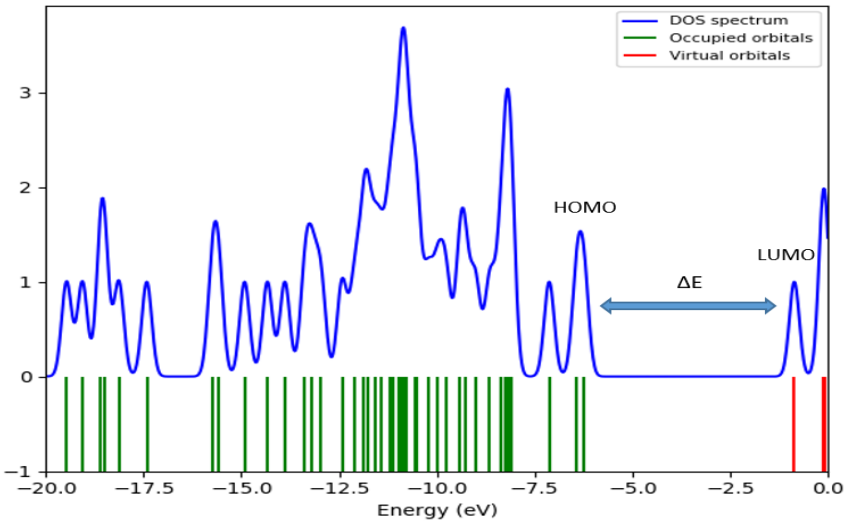

Figure 7. The density diagrams of compound 4.

The molecule with lower energy bandgaps are more polarizable and exhibit high reactivity [46]. Arrangement and energy levels of the orbitals, including HOMO and LUMO, determined by B3LYP/ cc-pVDZ for the current compound, are presented in Figure 6. The findings show that the greater energy level between HOMO and LUMO equals 5.378eV. All of the reactivity parameters of the compound are summarized in Table 5. Only HOMO and LUMO cannot be considered to provide a fair definition of frontier orbitals, as neighboring orbitals may display quasi-degenerate energy levels in the boundary region. For this reason, the gas phase and the density of states (DOS) were measured using the Gauss Sum 3.0 program, as shown in Figure 7.

Table 5. Electronic parameters of compounds 4.

B3LYP/ cc-pVDZ	Equations	Results
E_{LUMO+1} (eV)	E_{LUMO+1} (eV)	-0.115
E_{LUMO} (eV)	E_{LUMO} (eV)	-0.856
E_{HOMO} (eV)	E_{HOMO} (eV)	-6.235
E_{HOMO-1} (eV)	E_{HOMO-1} (eV)	-6.420
ΔE	HOMO - LOMO	5.378
I (eV)	$I= - E_{HOMO}$	6.235
A (eV)	$A= - E_{LUMO}$	0.856
X (eV)	X= I+A/2	3.546
η (eV)	η = I-A/2	2.689
μ (eV)	μ = -(I+A/2)	-3.546
S (eV)	S = 1/2η	0.185
ω (eV)	ω = μ2/2η	2.338

3.2.4. Molecular electrostatic potential (MEP) maps.

The molecule's molecular electrostatic potential (MEP) was calculated to predict reactive electrophilic and nucleophilic attack sites. At the molecule's surface, different colors represented the dissimilarity of the electrostatic potential. The potential increases from red to blue (red < orange < yellow < green < blue), the range map color started from -0.05367 a.u extreme red color to 0.05367 deepest blue color. MEP's positive (blue) regions are associated with electrophilic reactivity, and nucleophilic reactivity is related to the negative (red) areas. The MEP for the compound has a negative area based on the oxygen and a little bit on chlorine atoms presented in Figure 8. The maximum positive regions were located in the methyl and cyclobutane groups. The MEP has designated the negative sites as higher electronegative atoms and the positive sites as lower electronegativity atoms. The MEP surface shows that the C=O was strong repulsion to chlorine atom and reacted with electrophilic compounds.

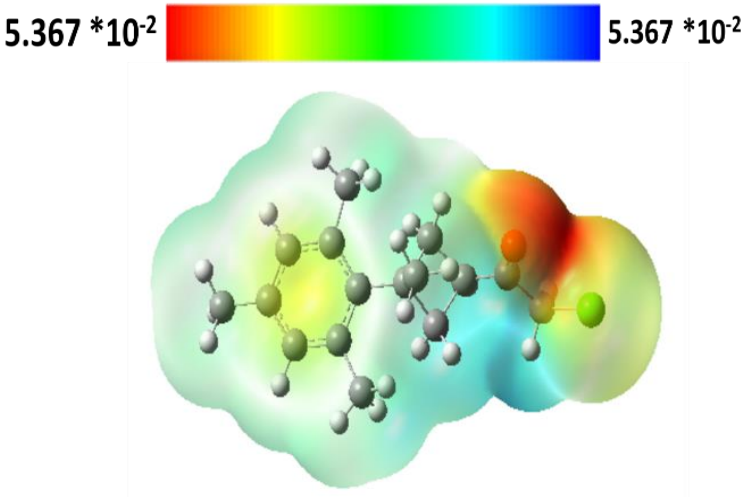

Figure 8. Molecular electrostatic potential (MEP) maps of compound 4.

3.2.5. Mulliken charge distribution.

The charge distribution on the molecule greatly influences the vibrational spectrum. The compound's molecular structure is composed of thirty-nine atoms: twenty-one hydrogens, sixteen-carbon, one oxygen, and one chlorine atom. The plot of the atomic charge distribution for the compound is presented in Figure 9. Generally, the hydrogen atoms of compound 4 were positive, while a small number of the carbon atoms with oxygen and chlorine atoms had a negative value. The carbon number 22, carbon for the cyclobutane ring, has a maximum negative value indicated to react with the more electrophilic compound. Also, oxygen 38 and chlorine 39 was negative peak values and reacted with electrophilic compounds.

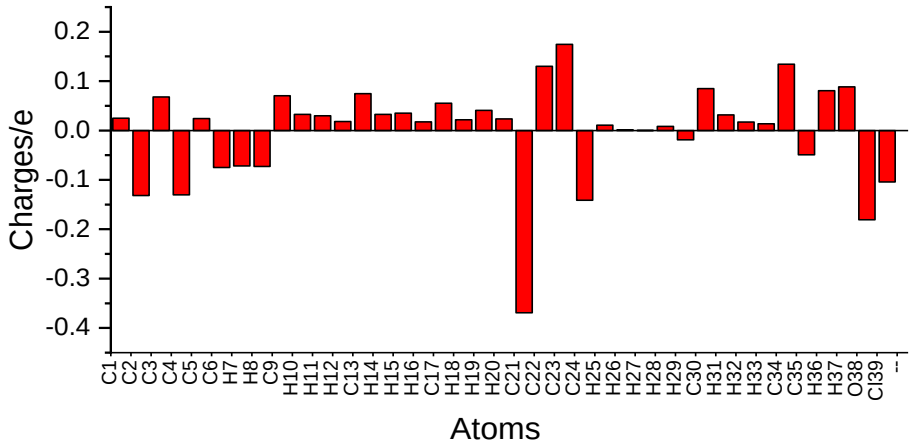

Figure 9. Mulliken charge distribution of compound 4.

3.2.6. Thermodynamic parameters.

The different thermodynamic properties of the molecule, including thermal energy, rotational temperatures, rotational constants, zero-point vibration energy, basic heat power, and entropy, were calculated based on B3LYP/cc-pVDZ at a pressure of 1.00 atom and 298 K, as summarized in Table 6.

Table 6. Thermodynamic parameters of compound 4.

Parameters	**B3LYP/cc-pVDZ**
Zero-point vibrational energy(kcal/mol^{-1})	206.805
Total energy (a.u.)	-1157.799
Rotational constants (GHz)	
	1.020
	0.155
	0.144
Rotational temperatures (K)	
	0.048
	0.007
	0.0069
Entropy (Kcal mol^{-1} K^{-1})	
Rotational	0.889
Translational	0.889
Vibrational	217.045
Total	218.823

4. Conclusions

2-chloro-1-(3-methyl-3-mesityl-cyclobutyl)–ethanone was successfully synthesized and characterized by FT-IR and NMR. The B3LYP/cc-pVDZ was used to analyze the theoretical calculations, including geometrical structure, electronic energy, vibrational motion,

and NMR. A comparison between theoretical and experimental results for FT-IR and NMR is founded. The study of the molecular reactivity was determined to form HMOM and LUMO energy levels. Molecular electrostatic potential (MEP) maps and Mulliken charge distribution show that the molecule has set for weak electronic interaction. Determining the thermodynamic properties was more important than knowing the structure reactivity of the molecule.

Funding

The research, authorship, and publication of this paper were not supported financially by the authors.

Acknowledgments

Tanks for Firat University, Chemistry Department to support this work.

Conflicts of Interest

There is no conflict of interest in this manuscript, according to the authors.

References

1. Scholz, S.O.; Kidd, J.B.; Capaldo, L.; Flikweert, N.E.; Littlefield, R.M.; Yoon, T.P. Construction of Complex Cyclobutane Building Blocks by Photosensitized [2+ 2] Cycloaddition of Vinyl Boronate Esters. *Organic Letters* **2021**, *23*, 3496-3501, https://doi.org/10.1021/acs.orglett.1c00938.
2. Horst, M.; Yang, J.; Meisner, J.; Kouznetsova, T.B.; Martínez, T.J.; Craig, S.L.; Xia, Y. Understanding the mechanochemistry of ladder-type cyclobutane mechanophores by single molecule force spectroscopy. *Journal of the American Chemical Society* **2021**, *143*, 12328-12334, https://doi.org/10.1021/jacs.1c05857.
3. Yilmaz, İ.; Çukurovali, A. Siklobütan Halkası İçeren Schiff Bazı ve Metal Komplekslerinin Sentezi ve Antimikrobiyal Aktivite Çalışmaları. *Avrupa Bilim ve Teknoloji Dergisi* **2019**, 437-444, http://dx.doi.org/10.31590/ejosat.621366.
4. Sepehri, B.; Ghavami, R.; Farahbakhsh, S.; Ahmadi, R. Machine learning-based quantitative structure–retention relationship models for predicting the retention indices of volatile organic pollutants. *International Journal of Environmental Science and Technology* **2022**, *19*, 1457-1466, https://doi.org/10.1007/s13762-021-03271-9.
5. Huang, Y.; Cohen, T.A.; Sperry, B.M.; Larson, H.; Nguyen, H.A.; Homer, M.K.; Dou, F.Y.; Jacoby, L.M.; Cossairt, B.M.; Gamelin, D.R. Organic building blocks at inorganic nanomaterial interfaces. *Materials Horizons* **2022**, *9*, 61-87, https://doi.org/10.1039/D1MH01294K.
6. Omar, R.; Koparir, P.; Koparir, M. Synthesis of 1, 3-Thiazole derivatives. *Indian Drugs* **2021**, *1*, http://dx.doi.org/10.53879/id.58.01.12427.
7. Rosen, T. The Perkin Reaction. *Comprehensive Organic Synthesis* **1992**, *2*, 395-408.
8. Akhmedov, M.; Sardarov, I.; Akhmedov, I.; Kostikov, R.; Kisin, A.; Babaev, N. Formation Of Substituted Cyclobutanes Under 2-(2-Methyl-2-Propenyl)-3-Chloromethyloxirane Interaction With Aromatic-Hydrocarbons. *Zhurnal Organicheskoi Khimii* **1991**, *27*, 1434-1440.
9. Koparir, P.; Rebaz, O.; Karatepe, M.; Ahmed, L. Synthesis, Characterization, and theoretical inhibitor study for (1E, 1'E)-2, 2'-thiobis (1-(3-mesityl-3-methylcyclobutyl) ethan-1-one) dioxime. *El-Cezeri* **2020**, *8*, 1495-1510, http://dx.doi.org/10.31202/ecjse.951527.
10. Koca, M.; Kirilmiş, C.; Arici, C. 1-(3-Mesityl-3-methylcyclobutyl)-2-phenoxyethanone. *Acta Crystallographica Section E: Structure Reports Online* **2010**, *66*, https://doi.org/10.1107%2FS1600536810003910.
11. Çukurovalı, A.; Özdemir, N.; Yılmaz, I.; Dinçer, M. 1-(3-Mesityl-3-methylcyclobutyl)-2-(piperidin-1-yl) ethanone. *Acta Crystallographica Section E: Structure Reports Online* **2005**, *61*, 1754-1756.
12. Dinçer, M.; Özdemir, N.; Çukurovalı, A.; Yılmaz, İ.; Büyükgüngör, O. 1-(3-Mesityl-3-methylcyclobutyl)-2-(pyrrolidin-1-yl) ethan-1-one. *Acta Crystallographica Section E: Structure Reports Online* **2004**, *60*, 1523-1524, http://dx.doi.org/10.1107/S1600536804019002.
13. Ahmed, L.; Rebaz, O. 1H-Pyrrole, Furan, and Thiophene Molecule Corrosion Inhibitor Behaviors. *Journal of Physical Chemistry and Functional Materials* **2021**, *4*, 1-4, https://doi.org/10.54565/jphcfum.989851.
14. Ahmed, L.; Rebaz, O. The Role of the Various Solvent Polarities on Piperine Reactivity and Stability. *Journal of Physical Chemistry and Functional Materials* **2021**, *4*, 10-16.

15. Anwar, R.; Koparir, P.; Qader, I.; Ahmed, L. Structure reactivity analysis for Phenylalanine and Tyrosine. *Cumhuriyet Science Journal* **2021**, *42*, 576-585, https://doi.org/10.17776/csj.881654.
16. Omer, R.A.; Ahmed, L.O.; Koparir, M.; Koparir, P. Theoretical analysis of the reactivity of chloroquine and hydroxychloroquine. *Indian Journal of Chemistry-Section A* **2020**, *59*, 1828-1834.
17. Lee, D.R.; Galant, N.J.; Wang, H.; Mucsi, Z.; Setiadi, D.H.; Viskolcz, B.; Csizmadia, I.G. Thermodynamic functions of molecular conformations of (2-fluoro-2-phenyl-1-ethyl) ammonium ion and (2-hydroxy-2-phenyl-1-ethyl) ammonium ion as models for protonated noradrenaline and adrenaline: first-principles computational study of conformations and thermodynamic functions for the noradrenaline and adrenaline models. *The Journal of Physical Chemistry A* **2009**, *113*, 2507-2515, https://doi.org/10.1021/jp807353n.
18. Sure, R.; Grimme, S. Corrected small basis set Hartree-Fock method for large systems. *Journal of computational chemistry* **2013**, *34*, 1672-1685, https://doi.org/10.1002/jcc.23317.
19. Ahmed, L.; Rebaz, O. Spectroscopic properties of Vitamin C: A theoretical work. *Cumhuriyet Science Journal* **2020**, *41*, 916-928, http://dx.doi.org/10.17776/csj.762184.
20. Omer, L.A.; Anwer, R.O. Population Analysis and UV-Vis spectra of Dopamine Molecule Using Gaussian 09. *Journal of Physical Chemistry and Functional Materials* **2020**, *3*, 48-58.
21. Anwar, R.; Koparir, P.; Qader, I.; Ahmed, L. Theoretical Determination of Corrosion Inhibitor Activities of Naphthalene and Tetralin. *Gazi University Journal Of Science* **2022**, *35*, 434-444, http://dx.doi.org/10.35378/gujs.888303.
22. Oelichmann, H.J.; Bougeard, D.; Schrader, B. Coupled calculation of vibrational frequencies and intensities: Part V. IR and Raman spectra of glyoxal and acrolein. *Journal of Molecular Structure* **1981**, *77*, 149-163, https://doi.org/10.1016/0022-2860(81)85277-5.
23. Jayaprakash, A.; Arjunan, V.; Jose, S.P.; Mohan, S. Vibrational and electronic investigations, thermodynamic parameters, HOMO and LUMO analysis on crotonaldehyde by ab initio and DFT methods. *Spectrochimica Acta Part A: Molecular and Biomolecular Spectroscopy* **2011**, *83*, 411-419, https://doi.org/10.1016/j.saa.2011.08.054.
24. Omer, L.A.; Rebaz, O. Computational Study on Paracetamol Drug. *Journal of Physical Chemistry and Functional Materials* **2020**, *3*, 9-13.
25. Rebaz, O.; Koparir, P.; Ahmed, L.; Koparir, M. Computational determination the reactivity of salbutamol and propranolol drugs. *Turkish Computational and Theoretical Chemistry* **2020**, *4*, 67-75, https://doi.org/10.33435/tcandtc.768758.
26. Gundelach, L.; Fox, T.; Tautermann, C.S.; Skylaris, C.-K. Protein–ligand free energies of binding from full-protein DFT calculations: convergence and choice of exchange–correlation functional. *Physical Chemistry Chemical Physics* **2021**, *23*, 9381-9393, https://doi.org/10.1039/D1CP00206F.
27. Sarkar, R.; Boggio-Pasqua, M.; Loos, P.-F.; Jacquemin, D. Benchmarking TD-DFT and wave function methods for oscillator strengths and excited-state dipole moments. *Journal of Chemical Theory and Computation* **2021**, *17*, 1117-1132, https://doi.org/10.1021/acs.jctc.0c01228.
28. Tao, X.; Yuan, D.; Zhang, N.; Jiang, M.; Shao, Z. Novel organic molecular second harmonic generation crystal: 3-methoxy-4-hydroxy-benzaldehyde. *Applied physics letters* **1992**, *60*, 1415-1417, https://doi.org/10.1063/1.107307.
29. Omer, R.A.; Koparir, P.; Ahmed, L.O. Characterization and Inhibitor Activity of Two Newly Synthesized Thiazole. *Journal of Bio-and Tribo-Corrosion* **2022**, *8*, 1-12, https://doi.org/10.1007/s40735-021-00625-1.
30. Koparir, P.; Sarac, K.; Omar, R.A. Synthesis, molecular characterization, biological and computational studies of new molecule contain 1, 2, 4-triazole, and Coumarin bearing 6, 8-dimethyl. *Biointerface Research in Applied Chemistry* **2022**, *12*, 809-823, https://doi.org/10.33263/BRIAC121.809823.
31. Omer, R.A.; Koparir, P.; Ahmed, L.; Koparir, M. Computational and spectroscopy study of melatonin. *Indian Journal of Chemistry-Section B (IJC-B)* **2021**, *60*, 732-741.
32. Liu, X.; Turner, C.H. Computational study of the electrostatic potential and charges of multivalent ionic liquid molecules. *Journal of Molecular Liquids* **2021**, *340*, https://doi.org/10.1016/j.molliq.2021.117190.
33. Moezi, E.; Mirzaei, M. Graphene scaffold for tioguanine delivery: DFT approach. *Lab-in-Silico* **2021**, *2*, 25-29.
34. Ahmed, L.; Omer, R.; Kebiroglu, H. A theoretical study on Dopamine molecule. *Journal of Physical Chemistry and Functional Materials* **2019**, *2*, 66-72.
35. Raj, R.; Gunasekaran, S.; Gnanasambandan, T.; Seshadri, S. Combined spectroscopic and DFT studies on 6-bromo-4-chloro-3-formyl coumarin. *Spectrochimica Acta Part A: Molecular and Biomolecular Spectroscopy* **2015**, *139*, 505-514, https://doi.org/10.1016/j.saa.2014.12.024.
36. Koparir, M.; Orek, C.; Koparir, P.; Sarac, K. Synthesis, experimental, theoretical characterization and biological activities of 4-ethyl-5-(2-hydroxyphenyl)-2H-1, 2, 4-triazole-3 (4H)-thione. *Spectrochimica Acta Part A: Molecular and Biomolecular Spectroscopy* **2013**, *105*, 522-531, http://dx.doi.org/10.1016/j.saa.2012.12.052.
37. Lin-Vien, D.; Colthup, N.B.; Fateley, W.G.; Grasselli, J.G. *The handbook of infrared and Raman characteristic frequencies of organic molecules*. Elsevier: **1991**.

38. Sarıkaya, E.K.; Dereli, Ö. Molecular structure and vibrational spectra of 7-Methoxy-4-methylcoumarin by density functional method. *Journal of Molecular Structure* **2013**, *1052*, 214-220, https://doi.org/10.1016/j.molstruc.2013.08.024.
39. Koparir, P.; Karaarslan, M.; Orek, C.; Koparir, M. Synthesis and in-vitro antimicrobial activity of novel aminophosphinic acids containing cyclobutane and 1, 3-thiazole. *Phosphorus, Sulfur, and Silicon and the Related Elements* **2011**, *186*, 2368-2376, https://doi.org/10.1080/10426507.2011.604660.
40. Moghanian, H.; Mobinikhaledi, A.; Monjezi, R. Synthesis, spectroscopy (vibrational, NMR and UV–vis) studies, HOMO–LUMO and NBO analysis of 8-formyl-7-hydroxy-4-methylcoumarin by ab initio calculations. *Journal of Molecular Structure* **2013**, *1052*, 135-145, https://doi.org/10.1016/j.molstruc.2013.08.043.
41. Koparir, P. Synthesis, antioxidant and antitumor activities of some of new cyclobutane containing triazoles derivatives. *Phosphorus, Sulfur, and Silicon and the Related Elements* **2019**, *194*, 1028-1034, https://doi.org/10.1080/10426507.2019.1597363.
42. Tammer, M.G. *Sokrates: Infrared and Raman characteristic group frequencies: tables and charts.* Springer: **2004**.
43. Sarıkaya, E.K.; Dereli, Ö.; Erdoğdu, Y.; Güllüoğlu, M. Molecular structure and vibrational spectra of 7-Ethoxycoumarin by density functional method. *Journal of Molecular Structure* **2013**, *1049*, 220-226, https://doi.org/10.1016/j.molstruc.2013.06.026.
44. Calais, J.L. *Density-functional theory of atoms and molecules*. Parr, R.G.; Yang, W. Oxford University Press, New York, Oxford, 1989. IX+ 333 pp. Price£ 45.00. Int. J. Quantum Chem. Volume 47, **1993**; pp.101-101, https://doi.org/10.1007/978-94-009-9027-2_2.
45. Gázquez, J.L. Perspectives on the density functional theory of chemical reactivity. *Journal of the Mexican Chemical Society* **2008**, *52*, 3-10.
46. Srivastava, K.; Shimpi, M.R.; Srivastava, A.; Tandon, P.; Sinha, K.; Velaga, S.P. Vibrational analysis and chemical activity of paracetamol–oxalic acid cocrystal based on monomer and dimer calculations: DFT and AIM approach. *RSC advances* **2016**, *6*, 10024-10037, https://doi.org/10.1039/C5RA24402A.